

LOW SPEED AERODYNAMICS OF SIX OPTIMISED UNCONVENTIONAL RE-ENTRY VEHICLE AEROSHAPES

Spartaco Massimo Giannino, Giuseppe Pezzella, & Antonio Viviani

Università della Campania "Luigi Vanvitelli", Dipartimento di Ingegneria. Via Roma 29, I-81031 Aversa (CE), Italy.

Abstract

This paper deals with the aerodynamic performances of several aeroshapes, developed for the optimal design of a multi-role crew return vehicle for low Earth orbit support services. The different configurations are the outcome of an in-house developed multidisciplinary design optimization procedure, aimed at providing unconventional blended wing bodies, with higher aerodynamic efficiency in comparison to conventional wing body spacecraft or blunt body capsules. The configurations under investigation differ from each other in the presence of vertical tails and /or winglets. However, each of these aeroshapes is characterized by a low aspect ratio double delta wing with positive dihedral and sweep angle. Furthermore, spacecraft aeroshapes exhibit a common set of specifications, including blunt shapes, flat windside, and low wingspan. It is evident that these features are very advantageous at hypersonic speeds, yet equally disadvantageous in low-speed flow conditions. Consequently, this research effort was focused on the subsonic aerodynamics of the aeroshapes, with the specific purpose of evaluating their landing capability on a conventional runway. Computational fluid dynamics analyses were carried out at Mach number less than 0.1 and at different angles of attack, with the objective of investigating the flow field that takes place past the optimal configurations. The aerodynamic performances are discussed in detail, with particular focus on the well-known vortex lift phenomenon and the associated lift increase, characterizing the double delta wing in the landing condition. The force and moment coefficients (i.e. C_L , C_D and $C_{M_{i-1}}$) are evaluated and an aerodynamic comparison between the vehicles analyzed is provided.

Keywords: Crew Return Vehicle, Blended Wing Body, Delta wing, Vortex lift, Vortex breakdown.

1. Introduction

The dismission of the Space Shuttle implied a growing demand for the development of a new generation of configurations suitable for space operations in Low Earth Orbit (LEO), i.e. support and service missions for the International Space Station (ISS). Actually, the current global landscape features a multitude of operational manned capsule configurations, like Soyuz, Shenzou and Crew Dragon developed in Russia, China and United States, respectively. This type of vehicles is featured by lower aerodynamic efficiency and maneuverability than Lifting Body (LB) or Blended Wing Body (BWB) aeroshapes. These latter exhibit a lower ballistic coefficient, which results in a more comfortable and safer re-entry. A figure of merit for this type of configurations is the Dream Chaser [1], [2], which is a reusable configuration developed by Sierra Nevada Corporation referring to the early NASA spaceplane concept well known as HL-20 [3].

At the same time, in the European context, the European Space Agency (ESA) is focusing on the development of the Space Rider [4], that will be an automated and reusable lifting body for unmanned re-entry, whose design is managed by the Centro Italiano Ricerche Aerospaziali (CIRA). The Space Rider will inherit the technology of the prototype Intermediate eXperimental Vehicle (IXV) [5], developed by ESA and tested in 2015 [6]. As previously stated, both the Dream Chaser and the Space Rider are reusable vehicles. Indeed, the configuration reusability is one of the leading requirements for this kind of spacecraft, since leads to a significant reduction in cost

and time between two following missions.

In this framework, the research main objective is the design of a reusable configuration able to perform support and service missions for the International Space Station (ISS), taking into account for all the specifications related to the speed regimes experienced during the whole re-entry flight. With this in mind, an in-house developed Multidisciplinary Design Optimization (MDO) [7], [8], [9] procedure was employed, in which a wide range of requirements that a re-enter vehicle must meet is considered. Particularly, the design is constrained in terms of maximum normal load factor, heat flux, dynamic pressure and landing velocity. In addition, several sub-disciplines, including aerodynamics, aerothermodynamics and flight mechanics, are considered in the MDO procedure. Due to the complexity of the problem, Low Order Fidelity tools (i.e. engineering-based tools) are used, resulting in a computational advantage during optimization process, where the best trade-off configurations are selected from thousands of potential options.

Finally, the objective functions exploited to identify the optimized aeroshapes are the minimum mass and maximum cross range. The latter represents a requisite condition, since the designers aim is to ensure that the configurations are able to land on a conventional runway. Therefore, to investigate the landing capability of the optimized blended wing body aeroshapes, the aerodynamic performances in low-speed conditions were evaluated with high-fidelity tools and experimental tests conducted in the "4 ft X 3 ft Low Speed Wind Tunnel" at the University of Sydney [10], [11]. In this work, the aerodynamic coefficients calculated using Computational Fluid Dynamics (CFD) simulations are compared for all configurations under investigation. In addition, the vortex lift and vortex breakdown phenomena, typical of delta wing planforms, are described. The objective of the forthcoming studies is to conduct a comparative analysis between the results obtained from CFD and those derived from Wind Tunnel (WT) experimental investigations. Therefore, the achieves presented in this paper concern a downscaled model and an upstream velocity of $30\ m/s$, to replicate the conditions observed in the WT tests [11].

1.1 Optimized configurations overview

The six aeroshapes obtained from the in-house developed MDO procedure are shown in Figure 1.

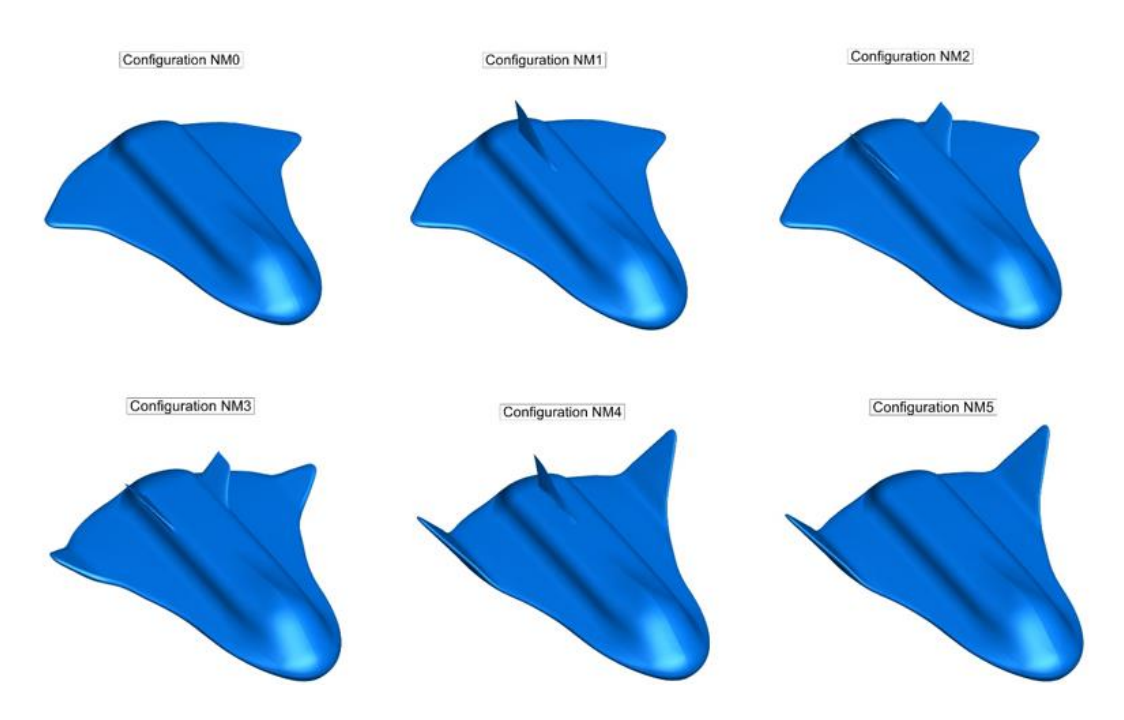


Figure 1 – Optimized aeroshapes under investigation.

As one can see, all the configurations exhibit an innovative BWB aeroshape, which enhances the aerodynamic performance (i.e., high lift-to-drag ratio, L/D) compared to conventional spacecrafts. In fact, the optimized aeroshape vehicles exhibit a lower ballistic coefficient, that in turn leads to decelerations at higher altitudes. The result is a reduction in heat flux peak, dynamic pressure and g-load, while simultaneously an increase in both range and cross-range. This implies an enhanced landing capability and a more comfortable re-entry for a potential crew. In addition, the flatbottomed side and the blunt shapes, which featured all the configurations, are two aspects necessary to promote heat dissipation at hypersonic speeds. However, the presence of rounded shapes leads to penalized aerodynamic efficiency at low-speed condition. All optimized vehicles exhibit the double-delta planform wing with a low aspect ratio. This is a highly advantageous design outcome of the MDO procedure, as it improves the aerodynamic performance of the vehicle in landing conditions, where high span wings are typically required. Indeed, in correspondence with the delta wing leading edge, a flow separation occurs, which subsequently gives rise to the formation of a primary, secondary and, in some instances, tertiary vortex [12]. This affects the vehicle aerodynamics with a resulting lift increase, known in literature as vortex lift phenomenon. The double delta wings also feature a positive dihedral angle, which enhances the lateral stability of the aircraft.

Finally, the vertical or butterfly tail of NM1, NM2, NM3 and NM4 configurations, and winglets of NM3, NM4, NM5 configurations, are useful design features which improve primarily the directional stability in comparison to the NM0 aeroshape (which does not exhibit any stabilizing aerodynamic surface). Therefore, the six layouts, being equipped with specific aerodynamic shape, represent the optimal trade-off configurations, which are consistent with the constraints due to all speed regimes experimented during the re-enter flight.

In this framework, the present research effort discusses the CFD results concerning the low-speed aerodynamic performance of NM0, NM1 and NM2 configurations (whose overall dimensions are reported in Table 1). As shown in Figure 1, the NM1 and NM2 configurations differ from NM0 one for the presence of a vertical tail and a butterfly tail, respectively.

The values presented in Table 1 for the "Reference length" and "Reference surface" represent the total length and the planform area of the configurations under investigation, respectively.

	Configuration NM0	Configuration NM1	Configuration NM2
Total height (H_t)	0.116 m	0.147 m	0.133 m
Reference length (L_{ref})	0.587 m	0.587 m	0.587 m
Half wingspan (b/2)	0.274 m	0.274 m	0.274 m
Reference surface (S_{ref})	$0.176 m^2$	$0.176 m^2$	$0.176 \ m^2$

Table 1 – Overall dimensions of NM0, NM1 and NM2 configurations.

2. Low speed aerodynamics

2.1 Computational grid

Flowfield simulations were carried out under symmetrical flow conditions and an Angle of Attack (AoA) variable between 0 and 35 degrees. As the longitudinal study for each configuration was conducted, three hybrid half-body grids were constructed, comprising tetrahedral cells in the outer flow and prisms in the boundary layer. Furthermore, a subdomain designated "density box" was defined around the spacecraft with the objective of increasing the number of elements within the regions of interest surrounding the vehicle body. This leads to a better description of the flow vortex system on the aeroshape leeside. In addition, the outer surfaces of the grid domain are located at sufficient distances from the vehicle body, that ensures the far field boundary condition is consistent.

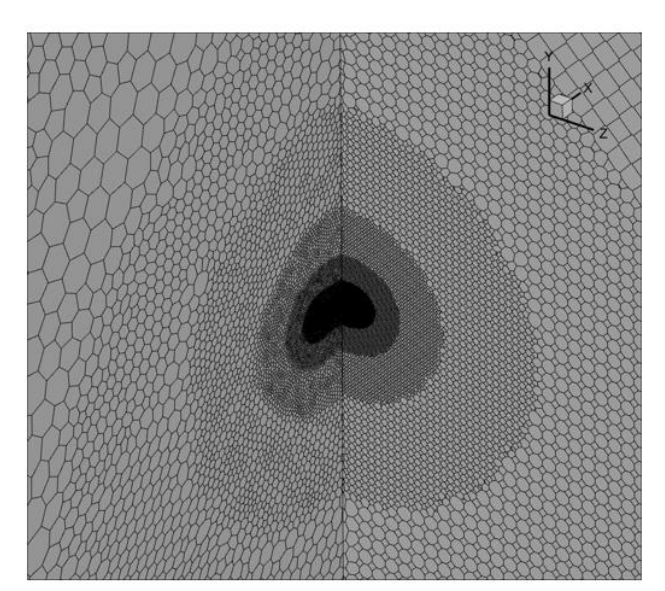
The grids exhibit a distance of the first cell from the aircraft surface equal to $5 \cdot 10^{-6} m$, ensuring a $y^+ = O(1)$, and a sufficient number of nodes to solve correctly the boundary layer. In fact, the boundary layer is discretized using 35 prismatic sublayers.

The numerical simulations were carried out taking advantage from the grid polyhedral conversion functionality available in Ansys Fluent [13]. This conversion process involves the polyhedral transformation of all tetrahedra elements, while the prismatic elements in the boundary layer are preserved.

The total number of mesh nodes and faces is approximately 13 million and 22 million, respectively. To provide an illustrative example, the mesh generated for NM0 configurations is presented in Figure 2. In particular, on the left side of the figure, the grid refinement near the configuration is visible, while on the right side, the unstructured surface mesh on the vehicle can be observed.

As one can see, the vehicle surface grid exhibits a heavy refinement near the wing leading edge where the flow separation occurs.

The aim of this work is to evaluate the integral aerodynamic force and momentum coefficients for each aeroshape. It is therefore expected that the results obtained with the unstructured grid are satisfactory. However, the future studies will provide a comparison between the outcomes obtained using a hybrid and structured grid, respectively. Furthermore, also a full-body grid will be generated to also investigate the lateral-directional performances of all the configurations.



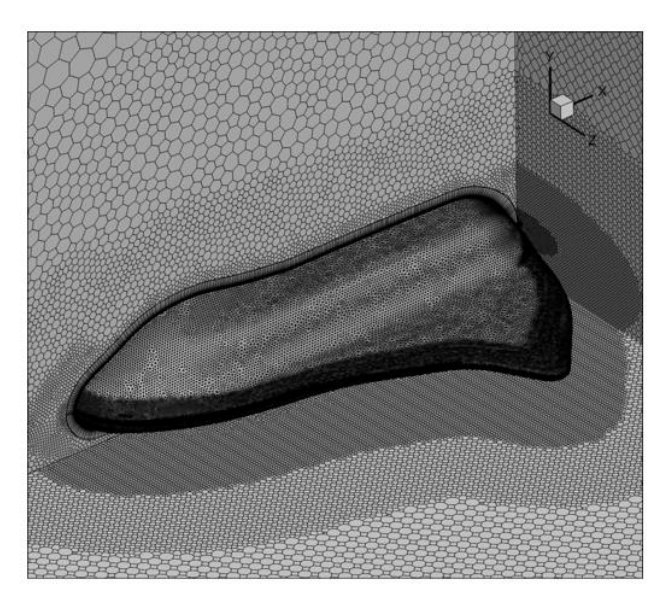


Figure 2 – Computational grid (NMO configuration).

2.2 Numerical settings

The numerical simulations were carried out solving the incompressible three-dimensional Reynolds Averaged Navier Stokes (RANS) equations, whose closure was realized using the Shear Stress Transport (SST) $k-\omega$ model [13]. In order to reproduce the WT test conditions, the free-stream velocity of 30 m/s was simulated at sea level conditions, resulting in a Mach number (M) of about 0.09 and Reynolds number (R_e) of $1.2 \cdot 10^6$.

Given the low Mach number, the steady, uncompressible coupled pressure-based solver was employed to resolve the system of continuity and momentum equations. Diffusive fluxes were discretized by using a second order accurate central-difference scheme, while convective ones by using second order upwind scheme.

The velocity inlet and pressure outlet boundary conditions were applied at the domain far field and outlet, respectively, while the symmetry condition was used at the domain face matching with the vehicle symmetry plane.

Finally, the aeroshape surface was considered as an adiabatic wall. CFD results presented hereafter were obtained through grid independent and converged steady state numerical simulations. The convergence was assessed according two criteria. Particularly, the numerical computations were considered converged, only when the equations residuals decreased by at least three order of magnitude and the aerodynamic coefficients reached a constant trend for a sufficient iterations number. The latter criterion is not satisfied at high angles of attack due to the vortex breakdown phenomenon, which results in a significant increase in flow unsteadiness. In this case, the convergence of the coefficients is evidenced by periodic trends, whose mean values were considered as results.

In future studies, unsteady CFD simulations will be conducted in order to achieve a more satisfactory description of the flowfield phenomena that affect the vehicles aerodynamic performances when the flow unsteadiness occurs.

2.3 Longitudinal aerodynamics

In this section the results obtained from numerical simulations are reported. For each configuration under investigation, the aerodynamic coefficients are normalized using the reference surfaces (S_{ref}) and length (L_{ref}) shown in Tab.1.

In particular, the aerodynamic forces coefficients (i.e., C_L and C_D) are evaluated in the wind axis reference frame, while the pitching moment coefficient ($C_{M_{\square}}$) is evaluated in the body axis system, in accordance with the ISO 1151 (see ref. [8]).

In the Figure 3, lift, drag, pitching moment (pole 45% L_t) coefficients and L/D ratio related to NM0 configuration are provided.

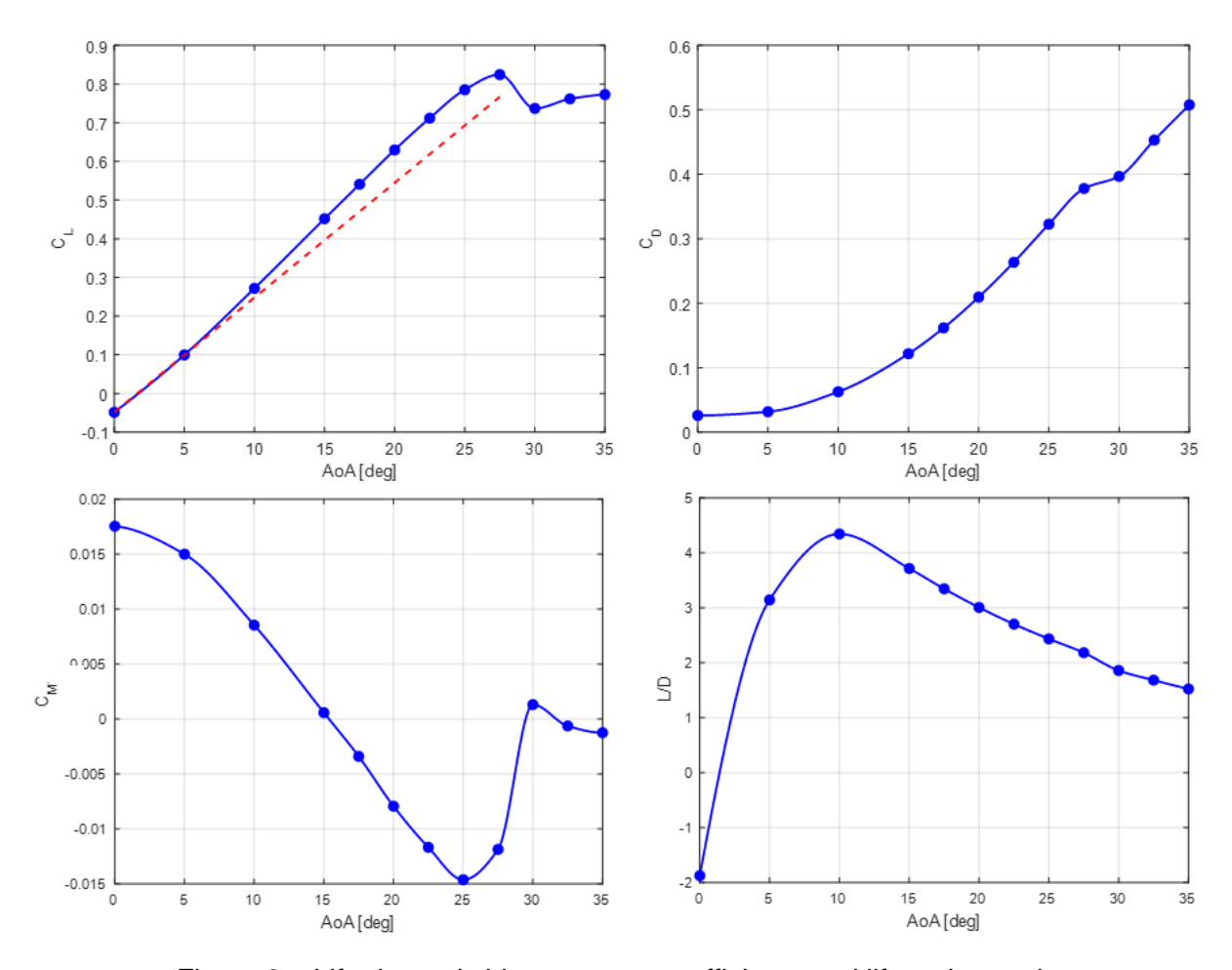


Figure 3 – Lift, drag, pitching moment coefficients and lift-to-drag ratio.

LOW SPEED AERODYNAMICS OF SIX OPTIMISED UNCONVENTIONAL RE-ENTRY VEHICLE AEROSHAPES

The pitching moment coefficient is evaluated with respect to a pole located at 45 % of the configuration total length, which is considered a reasonable center of gravity (CoG) position. As one can see, in the pre-stall condition, the vehicle is statically stable until to an attitude of 25° (with stability derivative C_{Ma} less than zero) and features a trim angle of about 15.4°.

In addition, the maximum aerodynamic efficiency is approximately 4.3, which is a relatively low value. This is attributed to the low aspect ratio wing and rather blunt aeroshape, which involve low lift and high drag, respectively. As one can see, the drag coefficient reaches values that are considerably higher than those typically observed for a conventional aircraft.

Finally, it is evident that at higher angles of attack, the linear trend of the lift coefficient is not preserved. In fact, an increase in the C_L curve slope, typical of the vortex lift phenomenon occurs [14]. Further clarification of this concept is provided in Figure 4, which depicts a comparison of the pressure coefficient (C_P) distribution on the NM0 configuration leeside (left side) and windside (right side) at angles of attack of 5° and 15°.

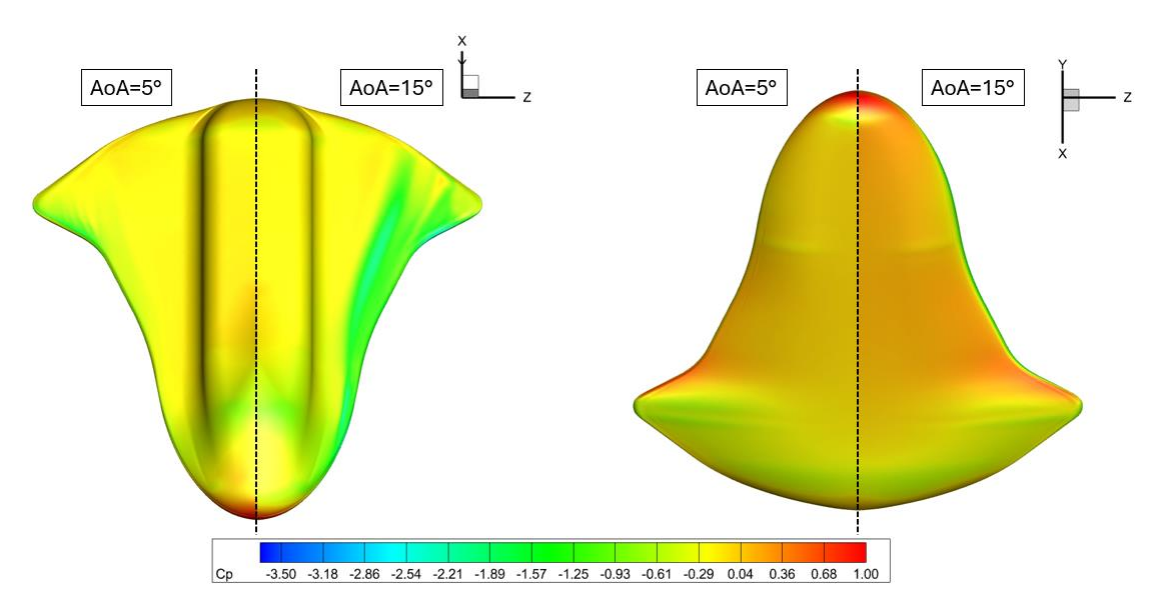


Figure 4 – Pressure coefficient on windside and leeside at AoA=5°,15° (NM0 configuration).

As one can see, at α =15°, the configuration exhibits a higher compression level on the windward side and a stronger expansion on the leeside, in the vicinity of the leading edges. The observed flow expansion is due to the vortex lift phenomenon. In fact, the difference in pressure between the windward and leeward sides leads to flow separation at the leading edge, which in turns results in the formation of vortex shedding.

The development of the vortex structures on the upper surface of the wing induces a flow acceleration with a subsequent decrease in static pressure, as illustrated in the Figure 4 (left side). As known, this turns in an enhanced suction level, which results in extra lift force and stall delay as pointed out by the trend of the lift coefficient showed in the Figure 3. In fact, the NM0 aeroshape exhibits a stall angle close to 27.5 degrees.

The primary and secondary counter-rotating vortices are developed on the upper surface of the configurations double delta wing [15], [16]. The influence of these vortices on the leeside pressure distribution is illustrated in the Figure 7. This figure shows the pressure coefficient trend on a cross-section located at $x=0.32 \, m$ from the vehicle nose.

In particular, the flow expansions resulting from the existence of the primary and secondary vortices are indicated. In the Figure 5, the presence of these two vortices is evidenced by the skin friction lines trend [17] on the surface body, where pressure coefficient distribution is also showed.

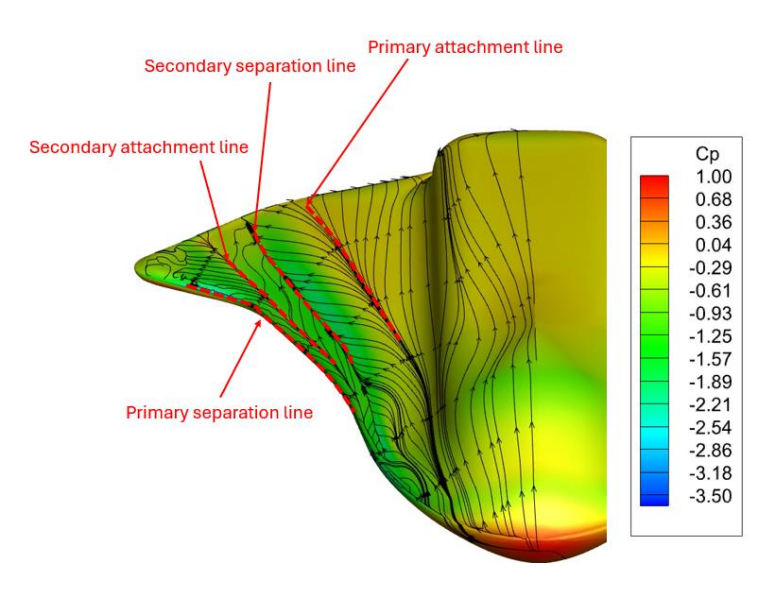


Figure 5 – Skin friction lines and pressure coefficient distribution for NM0 configuration (AoA=15°).

The primary separation line indicates the leading-edge point, at which flow separation occurs, resulting in the formation of a primary vortex and subsequent reattachment in correspondence with the primary attachment line. The primary vortex is continually sustained by the flow separation at the leading edge, exhibiting an external inviscid rotational region and an internal viscous core. The primary attachment line divides the undisturbed flow directed towards the trailing edge and the reattached flow, which is directed to the leading edge until it separates in correspondence with the secondary separation line. This results in the formation of a second vortex and a subsequent reattachment to the wing location corresponding to the secondary attachment line. The same conclusions can be derived from an analysis of the Figure 6, where the presence of the two vortices is investigated by using the Vorticity Magnitude contour (left side) and the Q-criterion iso-surfaces (right side). The Q-criterion iso-surfaces are associated with the pressure coefficient contour, thereby emphasizing that the maximum flow expansion occurs in correspondence with vortex flow.

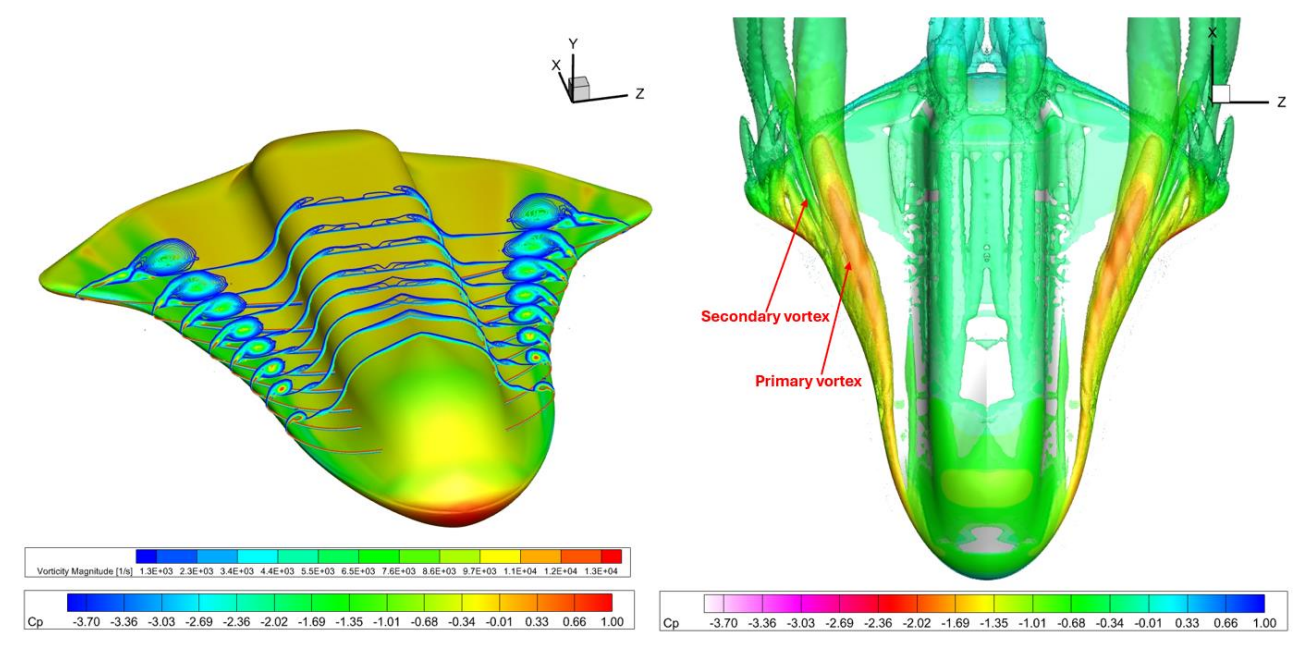


Figure 6 – Pressure distribution on body surface with vorticity magnitude at different cross sections (left side) and Q-criterion iso-surfaces with pressure contours (right side). Configuration NM0 at AoA=15°.

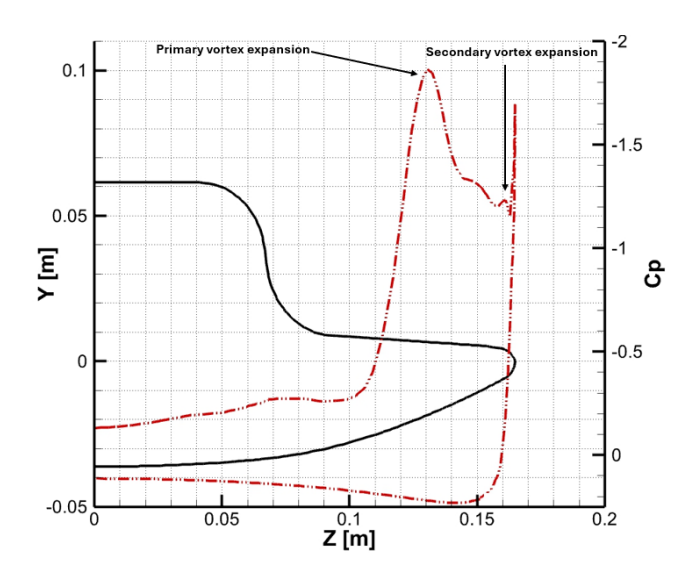


Figure 7 – Pressure coefficient distribution on a cross section (x=0.32 m).

As illustrated in the Figure 3, the lift coefficient exhibits a slower rate of increase at high attitudes, near the stall condition. Indeed, an increase in AoA leads to a corresponding change in the structure of the vortex flow. This phenomenon can be attributed to an instability of the primary vortex, which is associated with the adverse pressure gradient that occurs at elevated attitudes of the aircraft. When the wing incidence exceeds a critical value, the vortex core is characterized by a sudden expansion in a cross-sectional area, which is known as vortex breakdown or vortex bursting [18], [19]. There are several aspects that affect this flow phenomenon, such as the aircraft attitude (i.e. angle of attack and sideslip angle), asymptotic conditions, wing planform, et cetera. When the breakdown occurs, the axial velocity of the vortex core transits from jet to wake type, resulting in a considerable flow deceleration. The Figure 8 illustrates the pressure coefficient distribution and three-dimensional streamline trend for the NM0 configuration at α =22.5°, 27.5° and 32.5°. As one can see, the numerical results point out that the spiral breakdown [19] of the vortex moves forward (along the wing) as α increases, drastically affecting the aerodynamics of the configuration. In fact, downstream of the burst point, the flow expansion induced by the vortex flow disappears. Therefore, the greater the angle of attack, the smaller the wing region where the expansion due to the vortex lift phenomenon occurs. This, at very high incidences (i.e., 32.5°), results in a lower suction level and a consequent lift reduction, which leads to the wing stall condition. Figure 8 illustrates that, up to 32.5 degrees, the point of breakdown moves forward as the angle of attack increases, yet the vortex remains sufficiently stable near the wing apex. Indeed, in this region, an enhanced expansion level is observable as the AoA increases.

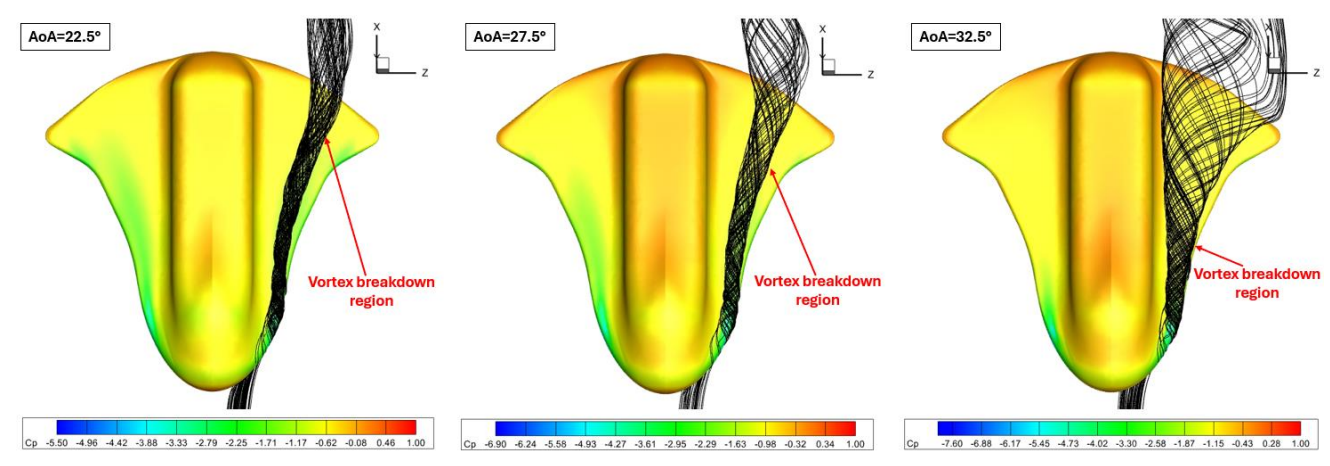


Figure 8 – Pressure distribution and 3D streamlines at α =22.5°,27.5° and 32.5°. NM0 aeroshape.

2.4 Results comparison

A comparative analysis of the longitudinal aerodynamic performance of all the configurations under investigation is presented. In particular, the Figure 9 illustrates the lift, drag, pitching moment coefficients and L/D ratio as a function of the AoA, α. The lift and drag coefficients exhibit a very similar trend across all the configurations in pre-stall conditions. This is due to the BWB low speed aerodynamics, which is significantly affected by the windside compression and wing leeside expansion (in turns, affected by the vortex breakdown). Conversely, the influence of the vertical and butterfly tail is minimal due to their significantly lower dimensions in comparison to that of the overall BWB. This is to be expected, as the stabilising surfaces have been designed by the authors to affect only the lateral-directional performances of vehicles. As can be observed, the pitching moment trends, related to a pole located at 45% L_{ref}, point out that all the configurations are longitudinally static stable in the pre-stall condition, with a trim angle of about 15.4 degrees for NM0/NM1 configurations and of 14.1 degrees for NM2 configuration. Obviously, the trim condition and stability levels will be discussed with more details in future works, where the full-scale model and a reasonable landing speed will be considered. The trend of aerodynamic coefficients indicates that the stall occurs at a smaller AoA (i.e., α =25°) for the NM2 configuration. This is attributed to the presence of the butterfly tail, which, due to its positioning, acts as an obstacle to the advancement of the flow. In fact, given the elliptical nature of the flowfield, the V-tail is the source of a disturbance that propagates instantaneously upstream. This affects the primary vortex dynamic, i.e. vortex breakdown phenomenon, with important influence on the stall condition.

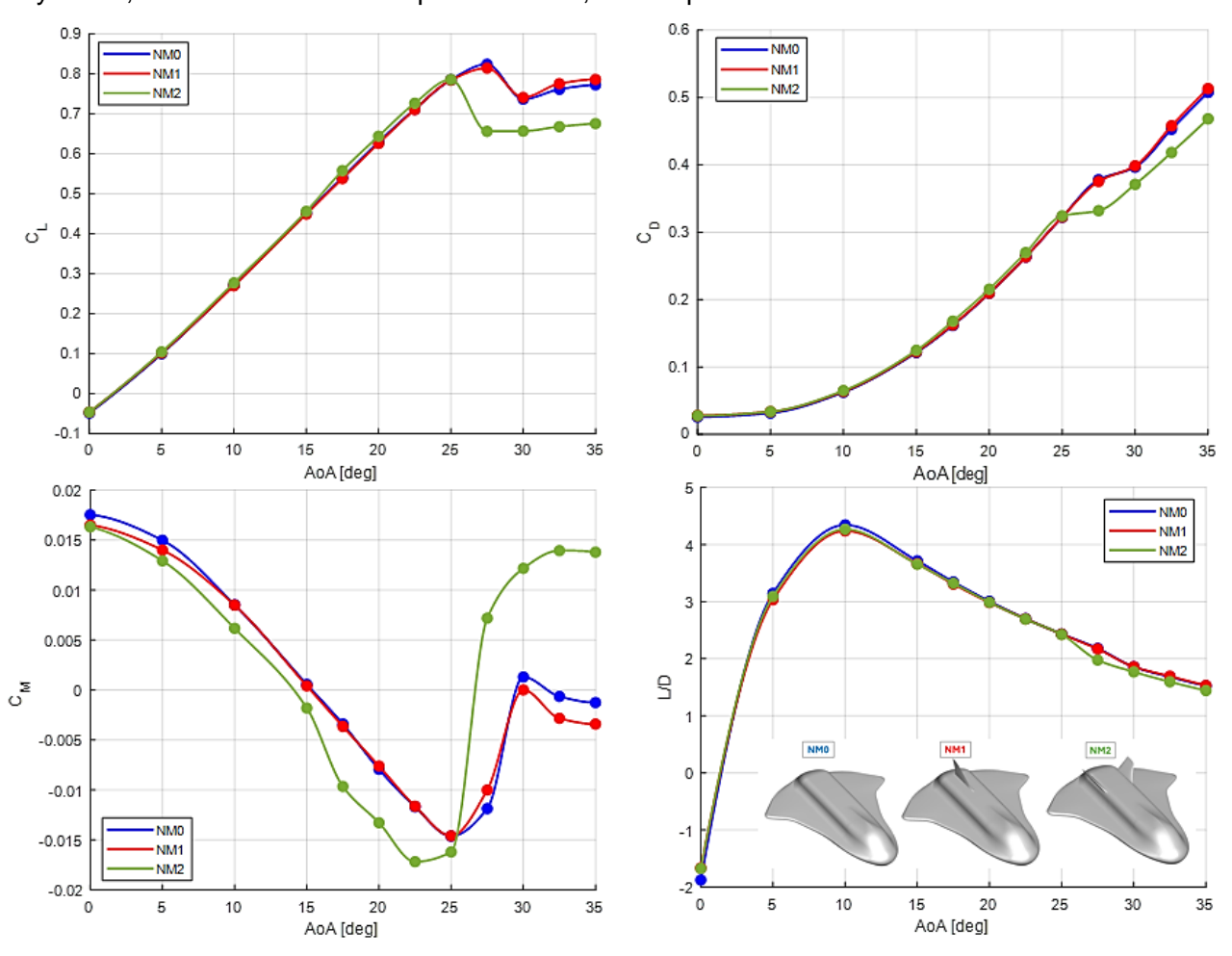


Figure 9 – Lift, Drag, pitching moment coefficient and lift to drag ratio comparison.

Figure 10, depicts the pressure coefficient distribution and a three-dimensional streamlines representation for both configurations NM1 and NM2 at α =27.5°. Given the similarity in the results

of the NM0 and NM1 configurations, for the sake of brevity, only the second one is shown in the aforementioned figure. The streamlines trend highlights that the spiral vortex breakdown occurs for both configurations. As previously stated, the spiral breakdown leads to a sudden reduction in the upper wing area, where the vortex lift expansion occurs. The described phenomenon is anticipated for the NM2 configuration (given the presence of the V-tail), with the vortex breakdown occurring at a more advanced wing station compared to NM1 configuration. This results in a different pressure distribution on the leeside of two vehicles, as showed in Figure 10 (right side). As one can see, the wing region, upstream vortex breakdown, is featured by a strong flow expansion, resulting in a pressure level that is considerably lower than that observed in the region downstream of the vortex bursting. Therefore, it's evident that at the considered AoA of 27.5 deg, the wing area, where the expansion due to vortex lift occurs, is significantly reduced in the NM2 configuration in comparison to the NM1 configuration. This results in an anticipated stall condition with a subsequent reduction in lift level for the configuration NM2. As expected, the butterfly tail affects only the aerodynamics of the configuration upper side, since the pressure distribution on the belly side of both NM1 and NM2 aeroshapes exhibits no relevant changes, as showed in Figure 11.

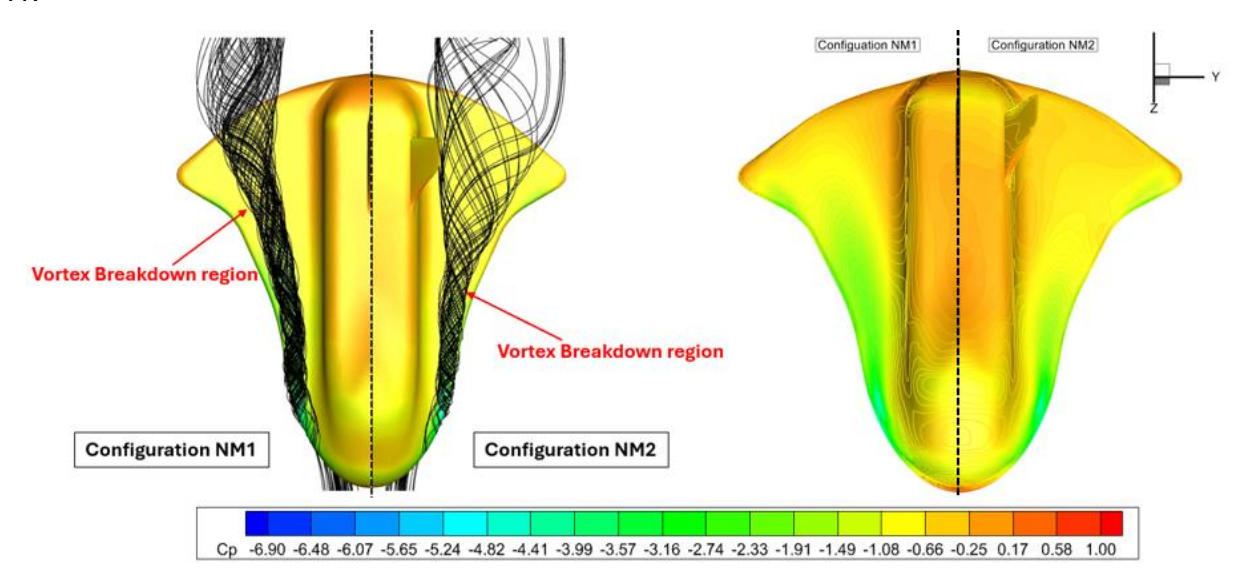


Figure 10 – 3D streamlines and pressure distribution comparison for NM1 and NM2 configurations.

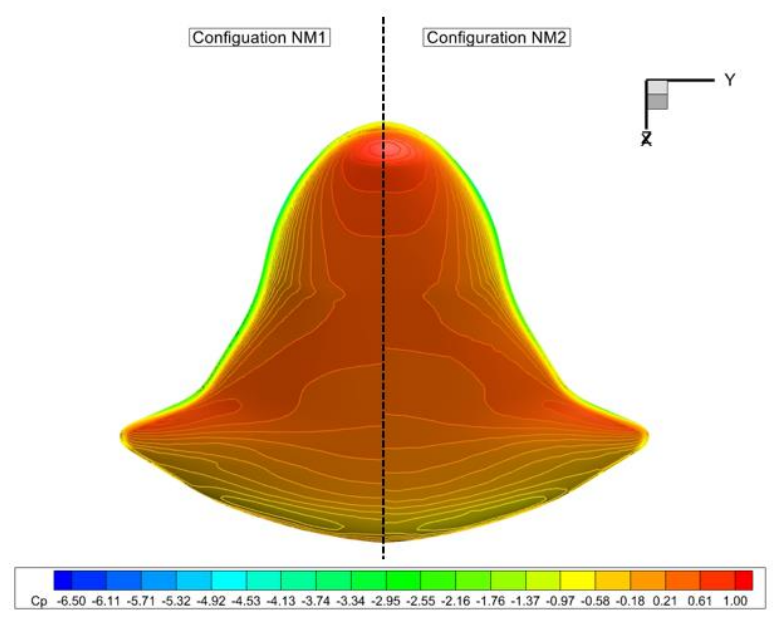


Figure 11 – Pressure distribution on the windside of NM1 (left side) and NM2 (right side) aeroshapes.

3. Conclusions

The present research effort dealt with the low-speed longitudinal aerodynamic performance of three distinct configurations, derived from a multidisciplinary optimization procedure. The studied aeroshapes exhibit specific aerodynamic features, that represent the optimal trade-off choices to satisfy the wide range of constraints due to the speed regimes experienced during re-entry flight. In order to evaluate the landing capability of the aforementioned vehicles, numerical flowfield simulations were conducted at low Mach number, considering a downscaled model to reproduce the same conditions of the wind tunnel tests. The results obtained point out that, as angle of attack increases, the aerodynamics of the double delta wing is featured by the development of two counter-rotating vortices, which are responsible of the vortex lift phenomenon. This results in an enhanced flow expansion, which in turn leads to a higher lift force. Therefore, the results obtained emphasize that the aerodynamics of the configurations is significantly affected by the double delta wing, which is precisely what the authors wanted to improve the performances of aeroshapes at landing conditions. In addition, it has been observed that the vortex breakdown phenomenon occurs at higher attitudes, affecting significantly the pressure distribution on the upper side of the wing. This subsequently leads to a reduction in the suction level, ultimately reaching the stall condition. Finally, the aerodynamic force coefficients trend comparison (i.e., C_L and C_D) indicates that the presence of the butterfly tail (featuring NM2 aeroshape) affects the aerodynamic performance of the configuration, inducing an anticipated stall condition at an angle of attack equal to about 25°. However, is expected that a viable landing attitude for the spacecraft under investigation, is within the range of 10° to 15°. At these incidences the longitudinal aerodynamic performance of the NM2 configuration is comparable to that of the NM0 and NM1 configurations. Furthermore, the presence of a butterfly tail could significantly improve the lateral-directional performance of the NM2 configuration. Hence, further numerical simulations will be conducted, introducing a sideslip angle, in order to evaluate the best trade-off aeroshape taking into account both longitudinal and lateral-directional performance. Obviously, this will be achieved by considering a full-scale model and an appropriate Mach number.

4. Contact Author Email Address

mailto: antonio.viviani@unicampania.it

5. Copyright Statement

The authors confirm that they, and/or their company or organization, hold copyright on all of the original material included in this paper. The authors also confirm that they have obtained permission, from the copyright holder of any third party material included in this paper, to publish it as part of their paper. The authors confirm that they give permission, or have obtained permission from the copyright holder of this paper, for the publication and distribution of this paper as part of the ICAS proceedings or as individual off-prints from the proceedings.

References

[1] «Dream Chaser Tenacity Uncrewed Cargo Spaceplane | Sierra Space (sierraspace.com),» [Online]. Available: https://www.sierraspace.com/dream-chaser-spaceplane/uncrewed-cargo-spacecraft/.

- [2] Howard, D. Russel e Z. Krevor, «Dream Chaser Commercial Crewed Spacecraft Overview,» in 17th AIAA International Space Planes and Hypersonic Systems and Technology Conference, San Francisco, CA., 2011.
- [3] «HL-20 SACD (nasa.gov),» [Online]. Available: https://sacd.larc.nasa.gov/vab/vab-projects/hl-20/.
- [4] «ESA To orbit and back with Space Rider,» [Online]. Available: https://www.esa.int/Enabling_Support/Space_Transportation/Space_Rider/To_orbit_and_back_with_Space_Rider.
- [5] Tumino G. e Yves G., «ESA Bulletin 128 IXV: the Intermediate eXperimental Vehicle.,» November 2006. [Online]. Available: https://www.esa.int/esapub/bulletin/bulletin128/bul128h_tumino.pdf.
- [6] G. Pezzella, G. Marino e G. Rufolo, «Aerodynamic Database Development of the ESA Intermediate Experimental Vehicle,» *ACTA ASTRONAUTICA*, vol. 94, n. 1, p. 57–72, 2014.
- [7] A. Aprovitola, L. Iuspa, G. Pezzella e A. Viviani, «Multidisciplinary Design of Reusable Re-Entry Vehicles by Optimization and Computational Fluid Dynamics,» in 8TH European Conference for Aeronautics and Space Sciences (EUCASS).
- [8] A. Viviani, A. Aprovitola, L. Iuspa e G. Pezzella, «Aeroshape design of reusable re-entry vehicles by multidisciplinary optimization and computational fluid dynamics,» *Aerosapce Science and Technology*, 2020.
- [9] L. Iuspa, A. Aprovitola, G. Pezzella, V. Cristillo e A. Viviani, «Multi-disciplinary optimization of a space re-entry vehicle using skeleton-based integral soft objects,» *Aerospace Science nad Technology*, 2022.
- [10] «Bykerk, T. USYD AMMEWind Tunnels. 2019.,» [Online]. Available: https://sites.google.com/view/usyd-amme-wind-tunnels/home.
- [11] N. Montella, Gareth Vio, L. Iuspa, A. Aprovitola, G. Pezzella e A. Viviani, «Wind Tunnel Analysis of A Space Re-entry Vehicle at Low-Speed Conditions,» in *34th Congress of the International Council of the Aeronautical Sciences (ICAS)*, Firenze, IT, 2024.
- [12] D. Sedlacek, S. Biechele e C. Breitsamter, «Numerical investigations of vortex formation on a generic multiple-swept-wing configuration,» *CEAS Aeronautical Journal*, 2022.
- [13] Ansys Fluent user's guide, 2021R1.
- [14] Edward C. Polhamus, «A CONCEPT OF THE VORTEX LIFT OF SHARP-EDGE DELTA WINGS BASED ON A LEADING-EDGE SUCTION ANALOGY,» National Aeronautics and Space Administration (NASA), 1966.
- [15] A. Viviani, A. Aprovitola, L. Iuspa e G. Pezzella, «Low speed longitudinal aerodynamics of a blended wing-body re-entry vehicle,» *Aerospace Science and Technology,* 2020.
- [16] A. Aprovitola, L. Iuspa, G. Pezzella e A. Viviani, «Phase-A design of a reusable re-entry vehicle,» *Acta Astronautica*, 2021.
- [17] A. Aprovitola, P. E. Di Nuzzo, G. Pezzella e A. Viviani, «Aerodynamic Analysis of a Supersonic Transport Aircraft at Landing Speed Conditions,» 2021.

LOW SPEED AERODYNAMICS OF SIX OPTIMISED UNCONVENTIONAL RE-ENTRY VEHICLE AEROSHAPES

- [18] C. Breitsamter, «Unsteady flow phenomena associated with leading-edge vortices,» *Progress in Aerospace Sciences.*
- [19] S. Gortz, «Realistic Simulations of Delta Wing Aerodynamics Using Novel CFD Methods».